

**A Diagnostic Study of the
Summer Southern Hemisphere Circulation of
the CCC General Circulation Model**

**Lin Su
C²GCR Report No. 91-20
December 1991**

**A Diagnostic Study of the
Summer Southern Hemisphere Circulation of
the CCC General Circulation Model**

Lin Su

A thesis submitted to the Faculty of Graduate Studies and
Research in partial fulfillment of the requirement for the degree
of Master of Science.

June, 1991
Department of Meteorology
McGill University
Montreal, Quebec, Canada

ABSTRACT

The medium scale planetary wave regime, consisting largely of zonal wavenumbers 5-7, frequently dominate the summer Southern Hemisphere tropospheric circulation. We perform a diagnostic study of this circulation as simulated by the Canadian Climate Centre (CCC) general circulation model (GCM). The analysis of Hovmoller diagrams, space-time and zonal wavenumber spectra shows that the CCC GCM is able to simulate the observed medium scale wave regime.

The zonally averaged meridional eddy heat and momentum transports and the associated baroclinic and barotropic energy conversions are also examined. The distributions of the transports on the vertical plane agree well with observations. When compared to the observed summer 1979 distributions, some quantitative differences remain: the vertical structure of the heat transport is too baroclinic, while the momentum transport tends to be too weak. The baroclinic and barotropic conversions all show a medium scale wave signal. The time evolution of the Richardson number of the mean flow suggests that the medium scale wave is due to a finite amplitude baroclinic instability.

RÉSUMÉ

Les ondes planétaires d'échelle moyenne, essentiellement les nombres d'onde 5-7, dominant fréquemment la circulation troposphérique estivale dans l'hémisphère sud. Nous effectuons une étude diagnostique de cette circulation telle que simulée par le modèle de circulation générale (MCG) du Centre Climatique Canadien (CCC). L'analyse de diagramme de Hovmöller, de spectres spatio-temporelles ainsi que de spectres des nombres d'onde zonaux démontre que le MCG est capable de simuler le mode des ondes d'échelle moyenne tel qu'observé.

Le transport méridional moyen, par bande de latitude, de chaleur et de quantité de mouvement ainsi que les transformations baroclines et barotropes d'énergie associées, sont étudiées dans ce mémoire. La distribution verticale de ces transports correspond bien aux observations. Toutefois, quelques différences quantitatives sont notées lorsque nous comparons nos résultats aux distributions observées durant l'été 1979. La structure verticale du transport de chaleur est trop barocline, tandis que le transport de quantité de mouvement est trop faible. Les transformations baroclines et barotropes démontrent tous un signal d'onde d'échelle moyenne. L'évolution dans le temps du nombre de Richardson du flux moyen suggère que les ondes d'échelle moyenne sont dues à des instabilités baroclines d'amplitude finie.

Acknowledgements

I wish to express my deepest gratitude to my thesis supervisor, Dr. C.A. Lin for his invaluable advice, patient guidance and indispensable support throughout my study.

I am grateful to Dr. J. Sheng for his valuable advice and helpful discussion during this work. I wish to thank Dr. S. Lambert of the Canadian Climate Centre, Atmospheric Environment Service, for providing results derived from NMC data, as well as helpful advice in this project.

I would also like to thank Mr. Alan Schwartz for technical help on computing, and Ms. Ursula Seidenfuss for drafting the figures.

Last but not least , I would like to thank my parents and my grandmother for all the support and understanding they have shown throughout my studies. I wish to dedicate this thesis to them.

TABLE OF CONTENTS

	Page
Abstract	i
Résumé	ii
Acknowledgements	iii
Table of contents	iv
List of figures	vi
List of tables	x
CHAPTER 1 : INTRODUCTION	1
CHAPTER 2 : CANADIAN CLIMATE CENTRE GENERAL CIRCULATION MODEL	4
CHAPTER 3 : EDDY GEOPOTENTIAL FIELD AND EDDY ENERGIES	6
3.1 : Hovmoller diagram and space-time spectra	6
3.2 : Eddy energies and interannual variability	15
CHAPTER 4 : EDDY TRANSPORTS AND ENERGETICS	22
4.1 : Zonally averaged heat and momentum	

	Page
transport	22
4.2 : Baroclinic and barotropic energy conversions	27
CHAPTER 5 CONCLUSIONS	36
APPENDIX	39
REFERENCES	43

List of Figures

FIGURE	PAGE
3.1: (a) A wavenumber 5 flow in the 200 mb height field (units of 100 m), as simulated by the CCC GCM on day 27, year 3. (b) The ECMWF IIIb 300 mb analyses (m) on February 9, 1979. (Adapted from Bjørheim et al. 1981)	7
3.2: Hovmoller diagrams of the 200 mb height eddy field (m) at 43°S for the 90-day period December-January -February (DJF) of year 3. (a) The total eddy component, (b) the TE component, and (c) the filtered TE component consisting of wavenumbers $m=4-7$. Shaded regions correspond to negative values.	8
3.3: As Figure 3.2, but at 500 mb.	9
3.4: The mean space-time height variance spectra (m^2) at 43°S, 200 mb for DJF of years 1-10. The scale is logarithmic, e.g. 2 denotes 100 m^2 . (a) The zonal wavenumber-period spectrum; E and W denote eastward and westward propagation respectively. (b) The latitude-period spectrum integrated over	

	Page
zonal wavenumbers $m=3-8$.	11
3.5: As Figure 3.4, but at 500 mb.	12
3.6: The zonal wavenumber height variance spectra for the TE (solid) and SE (dashed) components at 43°S , 200 mb, for DJF of years 2-7. The abscissa is the zonal wavenumber, and the ordinate is the height variance in units of 1000 m^2 ; (a)-(f) correspond to years 2-7 respectively.	13
3.7: As Figure 3.6, but at 500 mb.	14
3.8: The zonal wavenumber-latitude distributions of the zonal and height integrated EKE, in units of 10^4 J m^{-2} . (a) January 1979, (b) February 1983, and (c) March 1983; all from NMC analyses (Lambert, private communication). (d) The model simulated EKE for DJF of years 2-7.	16
3.9: The zonal wavenumber distribution of EKE (a), and EAPE (b) integrated from $5^{\circ}\text{S}-85^{\circ}\text{S}$, 1000-150 mb, for DJF of years 2-7 (solid). The observed distributions for summer of 1979 (January 1979 for	

- EKE from Lambert, 1986; DJF 1979 for EAPE from C87) are shown as the dashed lines. 19
- 4.1: The zonally averaged meridional eddy heat transport (K m s^{-1}) on the latitude-pressure plane. (a) Observed values for DJF 1979, taken from C87. (b) The model climatology for DJF of years 2-7. Negative values indicate poleward transport. 23
- 4.2: As Figure 4.1, but for the meridional eddy transport of westerly momentum ($\text{m}^2 \text{s}^{-2}$). 25
- 4.3: The model eddy conversions (10^{-2} W m^{-2}) integrated from 10° - 82°S , 1000-150 mb for years 2-7, as a function of the zonal wavenumber (m). (a) $C(\text{ZAPE}, \text{EAPE})$; (b) $C(\text{EAPE}, \text{EKE})$; and (c) $C(\text{EKE}, \text{ZKE})$. The solid and dashed lines denote the total eddy and TE contributions respectively, while the dots are observed values for DJF 1979, from C87. The dashed line is not shown in (a) as it is indistinguishable from the solid line. 29
- 4.4: The zonally averaged distributions of (a)

temperature (K), (b) zonal wind (m s^{-1}), and (c)

Richardson number (Ri), for DJF of years 2-7.

Values of Ri > 80 are not shown.

33

4.5: The time series for the upper tropospheric

Richardson number (Ri) minima, for DJF of model

year 2.

35

List of tables

Table	PAGE
3.1 The dominant zonal wavenumber of the wavenumber-latitude EKE spectrum of the CCC GCM, together with the magnitude of the maximum (10^4 J m^{-2}) and its latitude. Years "2-7" denotes the 6-year model climatology.	18
3.2 The total EKE and EAPE for DJF of years 2-7, and observed values from C87. The TE contributions to the total eddy energies are shown in brackets. The observed values from C87 also include the standard deviations over the period DJF 1979. The unit is 10^4 J m^{-2} .	21
4.1 The amplitudes of the lower and upper tropospheric maxima of the meridional eddy heat transport ($[\langle v'T' \rangle]$), and of the mid and high latitude momentum transport ($[\langle u'v' \rangle]$), for model years 2-7 and observed values from C87. Negative values indicate poleward transport.	26
4.2 Energy conversions for model years 2-7, and observed values from C87. The TE contributions to	

the total eddy conversion are shown in brackets.

The unit is 10^{-2} W m^{-2} .

Chapter 1. Introduction

Medium scale planetary waves, consisting largely of zonal wavenumbers 4-7, frequently dominate the summer Southern Hemisphere tropospheric general circulation. This signal has been well documented in the observational studies over the past decade. Salby (1982) first noted wavenumber 5 patterns are dominant in the temperature and geopotential fields during the summer months of FGGE, with maximum eddy amplitudes near the tropospheric jet core. The mode shows a regular eastward phase progression, with a period of about 11 days. The eddy structure suggests the mode is due to a baroclinic instability, with a sharp scale selection in both space and time. The same signal is also evident in the Southern Hemisphere total ozone, as observed by the Nimbus 7 Ozone Mapping Spectrometer during the FGGE observing period (Schoeberl and Krueger, 1983). Hamilton (1983), using a data set from the Australian Bureau of Meteorology, also noted a prominent wavenumber 5 peak in the 300 and 500 mb geopotential height fields in the Southern Hemisphere summer. In a series of observational studies, Randel and Stanford (1983, 1985a, 1985b, 1985c) identified a well defined eddy life cycle consisting of baroclinic growth to maturity and barotropic decay. Vacillations in wave-zonal mean exchange, with a time scale of 10-20 days, result from nonlinear baroclinic instability.

Lambert (1986) examined the eddy kinetic energy (EKE) budget of the summer Southern Hemisphere circulation during January 1979. There is a prominent peak in the EKE at wavenumber 5, and the dominant terms in the budget are the conversion of eddy available

potential energy (EAPE) to EKE, and EKE to zonal kinetic energy (ZKE). The energetics thus suggest the mode is indeed due to a baroclinic instability. Chen et al. (1987; hereafter referred to as C87) analyzed the same data set and showed that wavenumbers 4-6 account for half of the eddy momentum and heat transports. The developing stage of the waves are characterized by baroclinic processes and the decay stage by barotropic processes, again suggestive of a baroclinic instability. The authors speculated that Pacific sea surface temperatures might have an effect on the wave development, as the vertical structure of the eddy heat transport is modified when the wave passes over the ocean.

Although the existence of the medium scale waves in the summer Southern Hemisphere circulation is well documented, there have not been extensive modelling studies of this strong planetary wave signal. Kalnay and Mo (1986) performed experiments with a general circulation model to determine the origin of Southern Hemisphere stationary Rossby waves. In their "easterly deceleration" experiment, where the initial zonal flow is decelerated by adding a negative solid body rotation velocity of 5 m s^{-1} at the equator, a pentagonal stationary wave pattern is generated. They suggested that this might be related to the observed wavenumber 5 mode of the summer Southern Hemisphere. Lin and Chan (1989) used a 10-level linear quasi-geostrophic β -plane model to examine the baroclinic instability of the observed zonally and time averaged January 1979 zonal wind distribution. The fastest growing mode has a zonal wavelength corresponding to wavenumber 12 at 45°S . The mode corresponding to zonal wavenumber 5 is also baroclinically unstable

but with a smaller growth rate. Its latitude-height structure bears qualitative resemblance to the observed wavenumber 5 circulation. The latitude of the maximum eddy amplitude near 50°S is simulated, but the maximum is located near the surface instead of aloft. Full spherical geometry and nonlinear effects are likely to be important in the scale selection of the medium scale waves.

In this study, we diagnose the summer Southern Hemisphere planetary wave structure of the Canadian Climate Centre (CCC) general circulation model (GCM). As we saw earlier, observational studies suggest the wave is due to a finite amplitude baroclinic instability. It is thus of great interest to determine to what extent is the CCC GCM capable of simulating the wave regime. The next Chapter gives a brief description of the GCM. Chapter 3 examines the eddy geopotential field, and the eddy kinetic and available potential energies in the space-time domain. The eddy heat and momentum transports, and energetics are investigated in Chapter 4. The concluding remarks are presented in the final chapter.

Chapter 2. Canadian Climate Centre general circulation model

The CCC GCM is described in detail by Boer et al. (1984a). We give here a brief description of its various features. The model governing equations are the primitive equations of motion, which explicitly resolve the major physical processes that produce weather and climate. Sub-grid scale processes are parameterized using stability dependent eddy diffusivities and bulk transfer coefficients. A parameterization of the momentum transport induced by topographic gravity waves is included. The computation of radiation includes both the annual and diurnal cycles. The model variables are represented in the horizontal by a spectral formulation using spherical harmonics with twenty zonal wavenumbers and a triangular truncation. Vertical derivatives are approximated using finite differences. The vertical coordinate is $\sigma = p/p_s$, where p and p_s are the pressure and surface pressure respectively. Twelve σ levels at $\sigma = 0, 0.010, 0.032, 0.080, 0.150, 0.235, 0.360, 0.550, 0.750, 0.880, 0.970, 1.00$ are used. Other features of the numerics include the use of semi-implicit time stepping and a weak time filter. The topographic heights of the major land masses are prescribed. Land and ice surface temperatures are calculated from a surface energy balance. Sea surface temperatures are prescribed using monthly climatological means.

In a companion study, Boer et al. (1984b) showed the model climatology is quite close to that of the atmosphere. Time mean fields of zonal wind, temperature, mean meridional circulation, specific humidity, eddy kinetic energy, mean sea level pressure,

precipitation rate, 500 mb height field generally compare well with observed values in the troposphere.

Xu et al. (1990) analyzed the performance of 4 GCM's in the Southern Hemisphere, one of which is the CCC model. The other models are those of National Center for Atmospheric Research (NCAR), European Centre for Medium Range-Weather Forecasts (ECMWF), and Geophysical Fluid Dynamics Laboratory (GFDL). The main focus of their study was on the semiannual wave, and they did not address the medium scale wave regime, which is the primary focus of this work.

The data set used in this study consists of 10 years of model simulation. We refer to the period covered by the model data set as years 1-10.

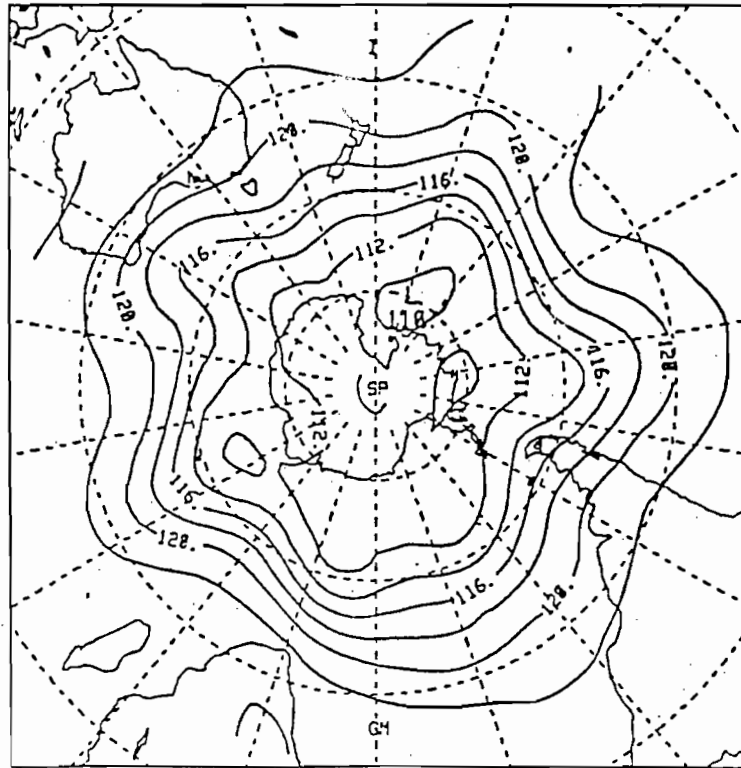
Chapter 3. Eddy geopotential field and energies

3.1 Hovmoller diagrams and space-time spectra

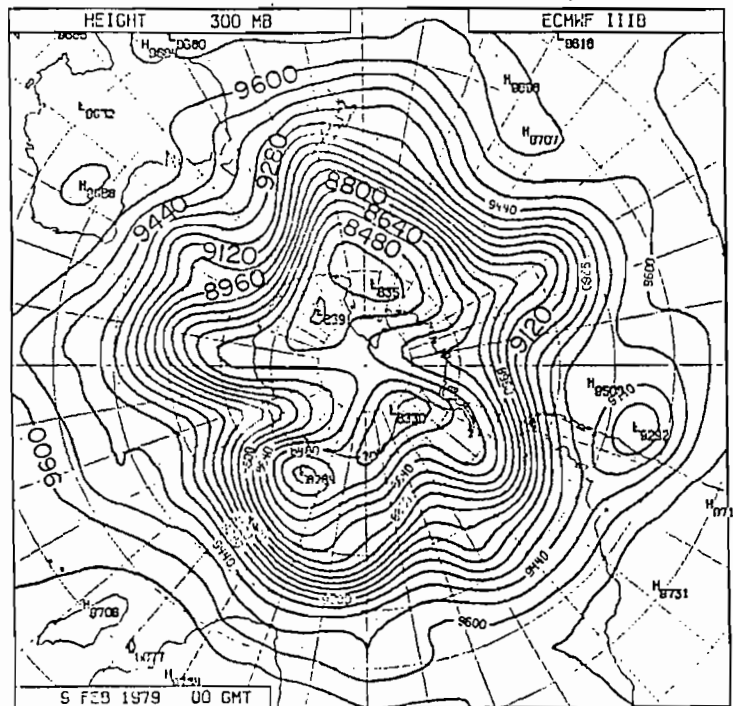
The medium scale waves in the summer Southern Hemisphere have maximum amplitude in the upper troposphere at mid-latitudes. Figure 3.1 shows an example of a flow consisting predominantly of zonal wavenumber $m=5$ in the 200 mb geopotential height field, as simulated by the model on day 27, year 3. For comparison, the observed 300 mb height field on February 9, 1979 is also shown. We see a pentagonal feature dominating both flows at these particular times. To further examine the propagation properties of the wave, we decompose the height field (z) into time and zonal mean ($[\langle z \rangle]$), stationary eddy (z^*), and transient eddy (z') components.

$$z = [\langle z \rangle] + z^* + z'$$

Time and zonal means are denoted by $[]$ and $\langle \rangle$ respectively, while superscripts $*$ and $'$ denote departures from the respective time and zonal means. The stationary eddy (SE) and transient eddy (TE) components together will be referred to as the eddy component. Henceforth, we use m to denote the zonal wavenumber. In Figure 3.2, we show Hovmoller diagrams of the year 3 height field at 200 mb, 43°S , of the eddy component, the TE component, and the filtered $m=3-7$ contribution to the TE component. We see from the eddy field that there is a significant stationary component in the first half of the 90-day simulation; the latter covers the December-January-February (DJF) period. C87 suggested that the change in the nature of the propagation to a quasi-stationary wave might be related to



(a)



(b)

Figure 3.1: (a) A wavenumber 5 flow in the 200 mb height field (units of 100 m), as simulated by the CCC GCM on day 27, year 3. (b) The ECMWF IIIB 300 mb analyses (m) on February 9, 1979. (Adopted from Bjornheim et al. 1981.)

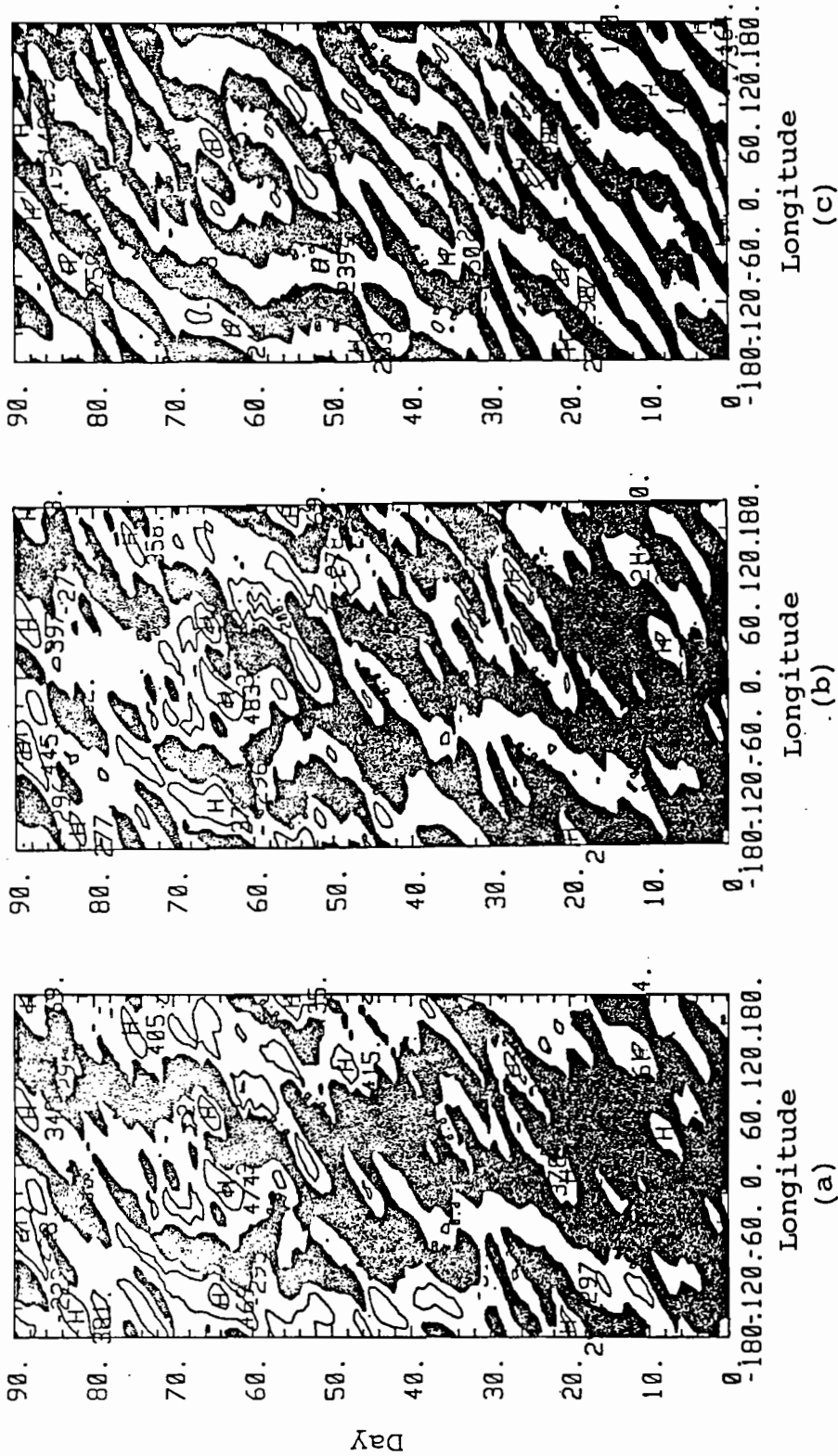


Figure 3.2: Hovmöller diagrams of the 200 mb height eddy field (m) at 43°S for the 90-day period December-February (DJF) of year 3. (a) The total eddy component, (b) the TE component, and (c) the filtered TE component consisting of wavenumbers $m=4-7$. Shaded regions correspond to negative values.

the onset of the Southern Hemisphere monsoon. Both the TE and the filtered TE components show clear eastward propagation of the planetary wave with a period of about 10 days, in good agreement with the observations. The amplitude of the filtered TE component is over half of that of the total TE flow, thus showing the importance of the medium scale wave regime. The presence of this wave regime is also evident at the 500 mb level, but with reduced amplitudes (Figure 3.3).

The space-time spectrum method and their applications were reviewed by Hayashi(1982). In this study, the space-time spectra were calculated by the direct Fourier transform method. The length of the time record is 120 outputs, equivalent to 90 days out of each year.

The propagation characteristics and latitudinal structure of the wave are shown by the DJF 10-year mean space-time height spectra ($\langle z^2 \rangle$) at 200 mb (Figure 3.4). In Figure 3.4(a,b), for x-axis the unit is days on the bottom of both plots, and frequency (day^{-1}) at the top. For the y-axis, the unit is wavenumber for Figure 3.4a, and latitude for Figure 3.4b. The zonal wavenumber-period spectrum shows the presence of eastward moving waves of zonal wavenumbers $m=3-8$. The latitudinal distribution of these waves shows a well defined maximum in the eddy amplitude near $45-50^\circ\text{S}$ with eastward propagation. The medium scale wave regime with period of about 10 days merges into the longer period low frequency variability modes. Evidence of the wave regime is present at 500 mb as well, but with a reduced amplitude (Figure 3.5).

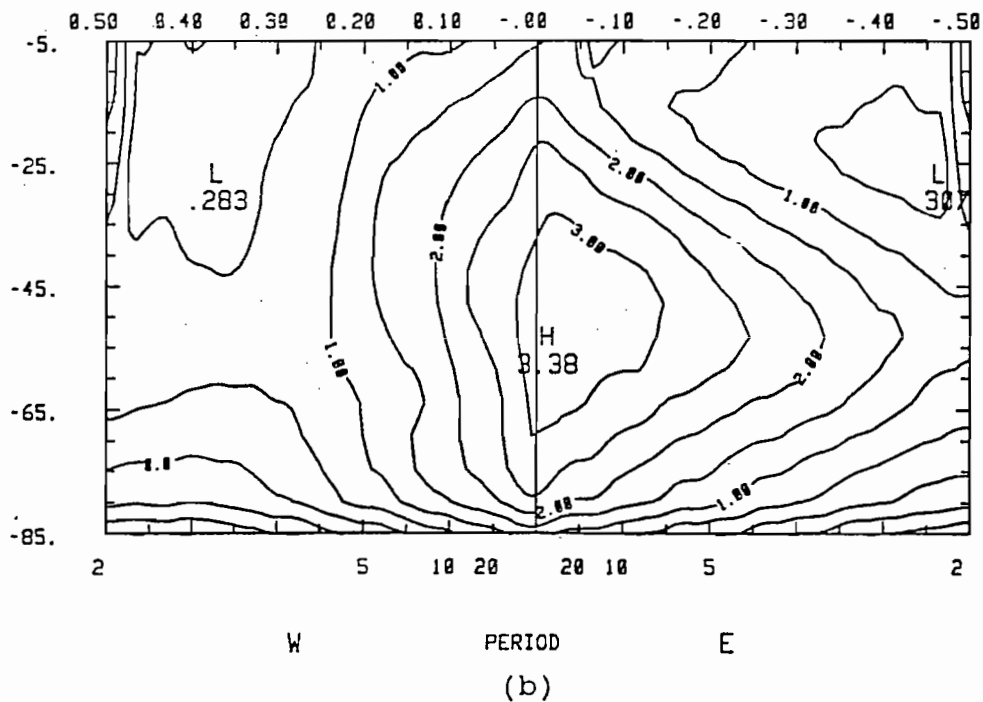
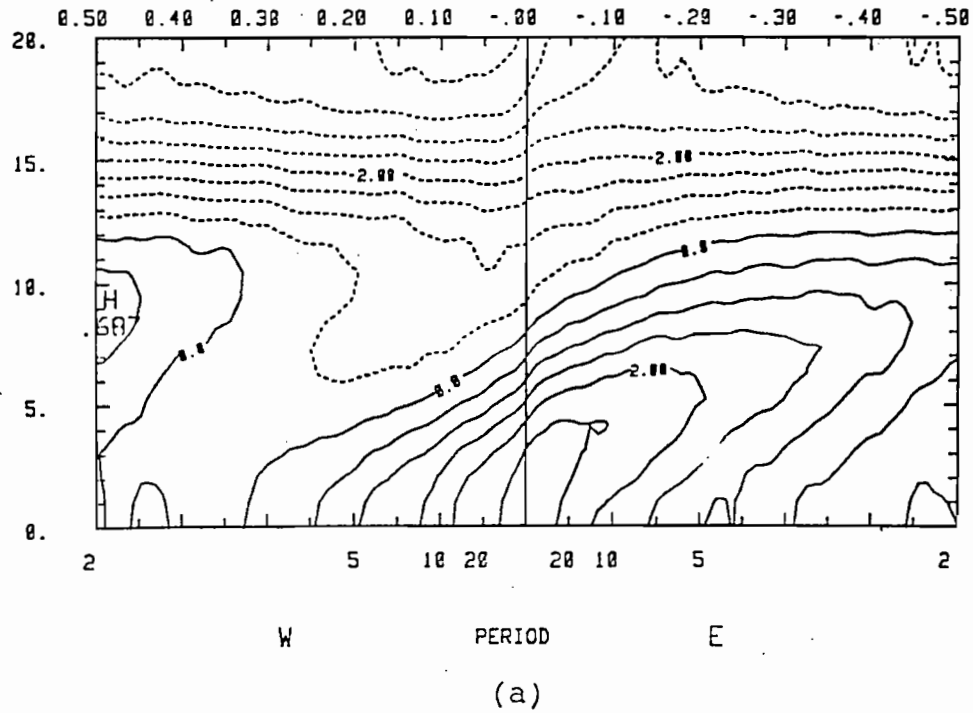


Figure 3.4: The mean space-time height variance spectra (m^2) at $43^\circ S$, 200 mb for DJF of years 1-10. The scale is logarithmic, e.g. 2 denotes $100 m^2$. (a) The zonal wavenumber-period spectrum; E and W denote eastward and westward propagation respectively. (b) The latitude-period spectrum integrated over zonal wavenumbers $m=3-8$.

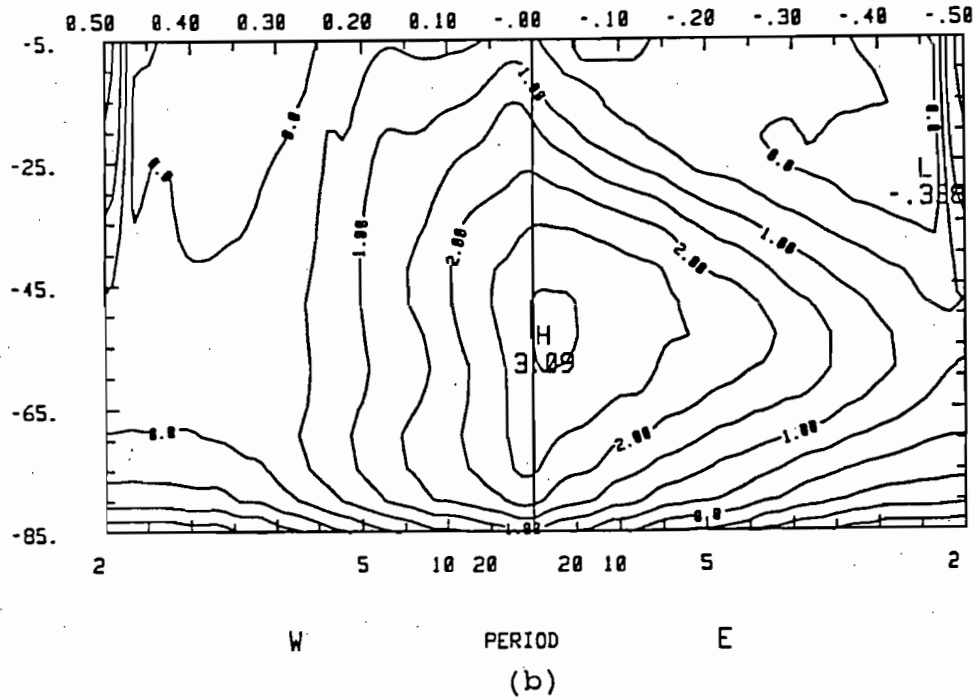
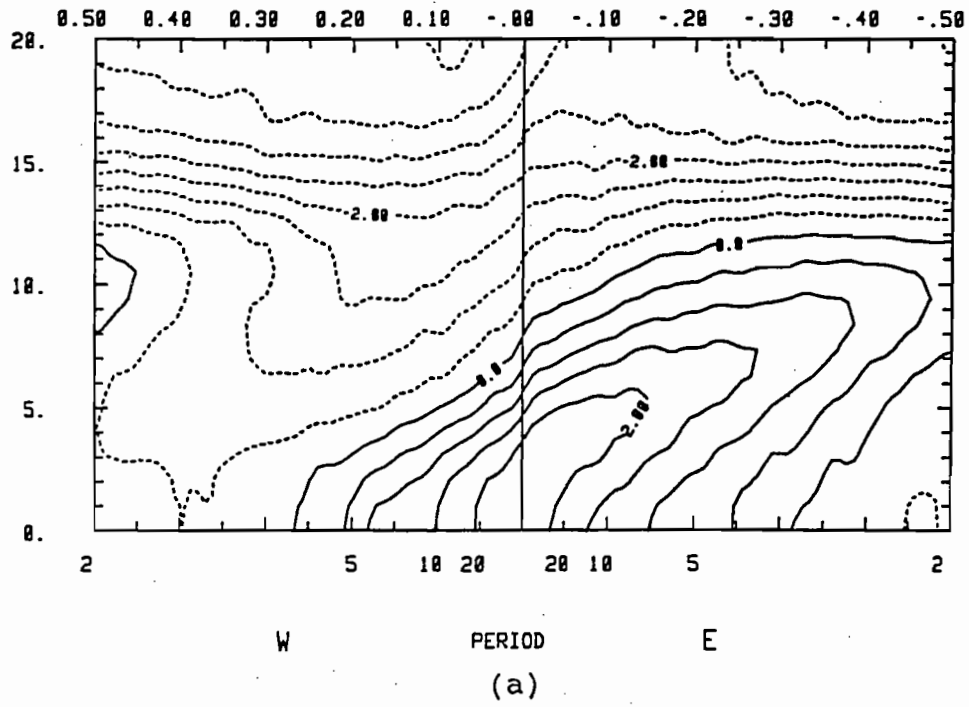


Figure 3.5: As Figure 3.4, but at 500 mb.

We next examine the zonal wavenumber height variance spectra of the SE ($[\langle z^* \rangle^2]$) and TE ($\langle z'^2 \rangle$) components. Figure 3.6 shows the spectra at 200 mb and 43°S for the summer months of December, January and February, for years 2-7. These two components form part of the total height variance ($[\langle z^2 \rangle]$) examined earlier.

$$[\langle z^2 \rangle] = [\langle z \rangle]^2 + [\langle z^* \rangle^2] + [\langle z'^2 \rangle]$$

We see that in almost all cases, the amplitude of the TE component exceeds that of the SE's, with the zonal wavenumbers $m=3-7$ being most prominent. The latter is sometimes present as a broad maximum (e.g., December of year 3), or it can be a sharp maximum at a specific wavenumber (e.g., wavenumber 4 in January of year 4). The SE contribution to the variance is due primarily to zonal wavenumbers $m=1$ and $m=3$. This agrees with the result of Xu et al. (1990), who showed that in the CCC GCM, these two wavenumbers account for almost all the stationary variance at about 45°S . The corresponding height spectra at 500 mb are shown in Figure 3.7. The signal of the medium scale waves is weaker at this level, but the wave regime is still discernible.

3.2 Eddy energies and interannual variability

Lambert (1986) evaluated the zonal wavenumber/latitude distribution of the vertically averaged EKE, using the FGGE data for the January 1979; there is a clear $m=5$ signal for this month. However, different zonal wavenumbers can develop at other times. Figures 3.8 (a) - (c) (Lambert, private communication) show the

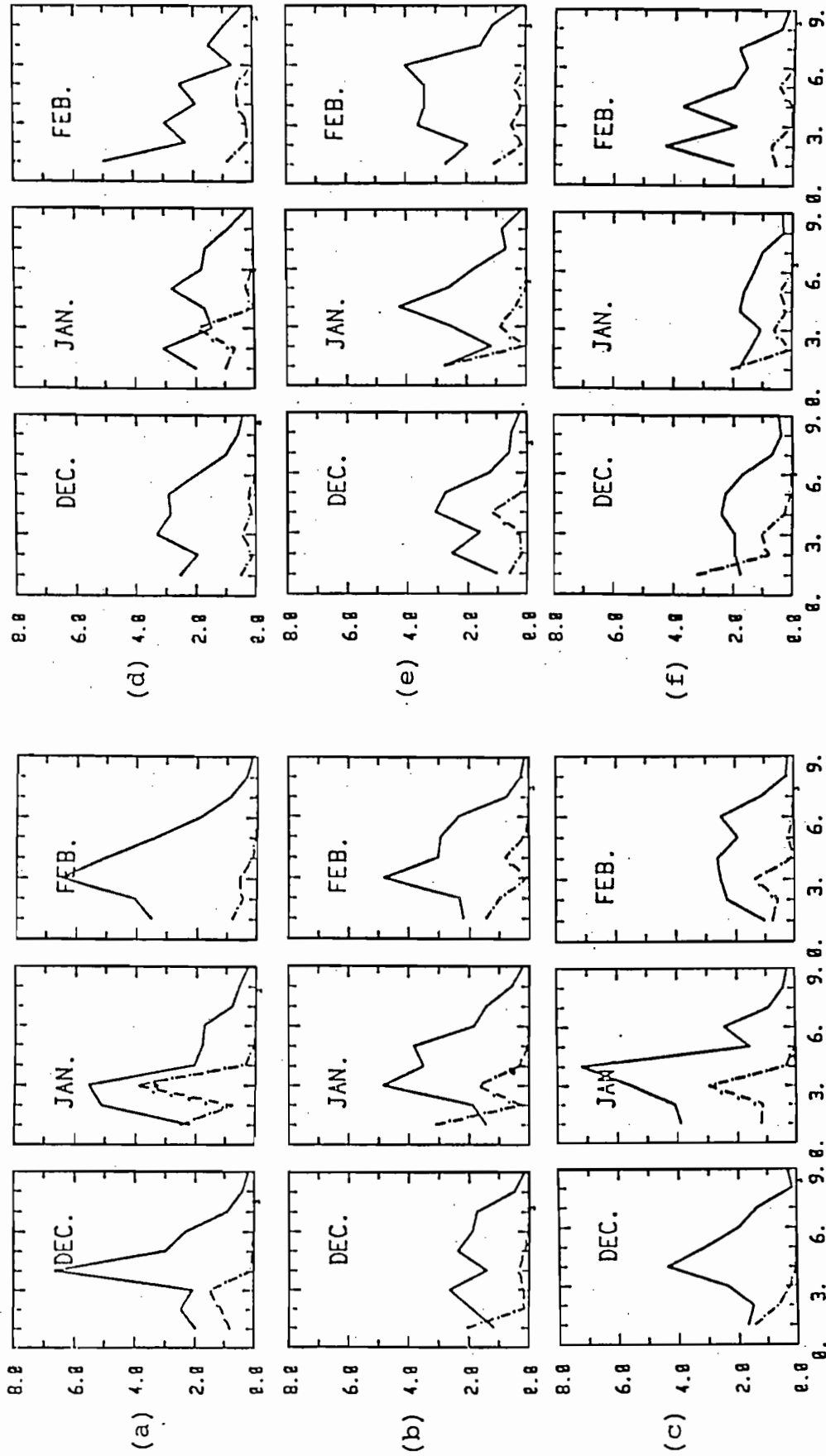


Figure 3.6: The zonal wavenumber height variance spectra for the TE (solid) and SE (dashed) components at 43°S, 200 mb, for DJF of years 2-7. The abscissa is the zonal wavenumber, and the ordinate is the height variance in units of 1000 m²; (a)-(f) correspond to years 2-7 respectively.

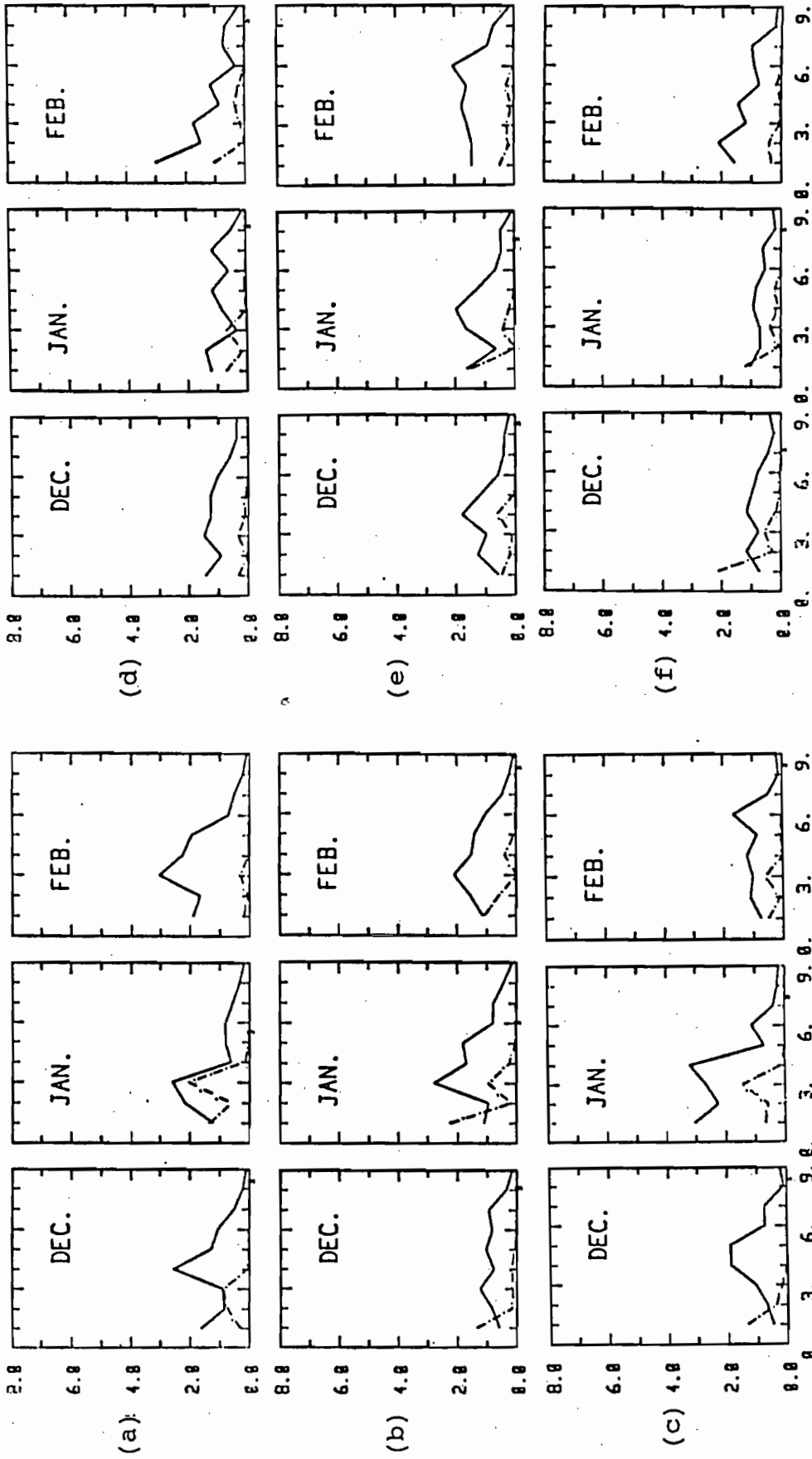


Figure 3.7: As Figure 3.6, but at 500 mb.

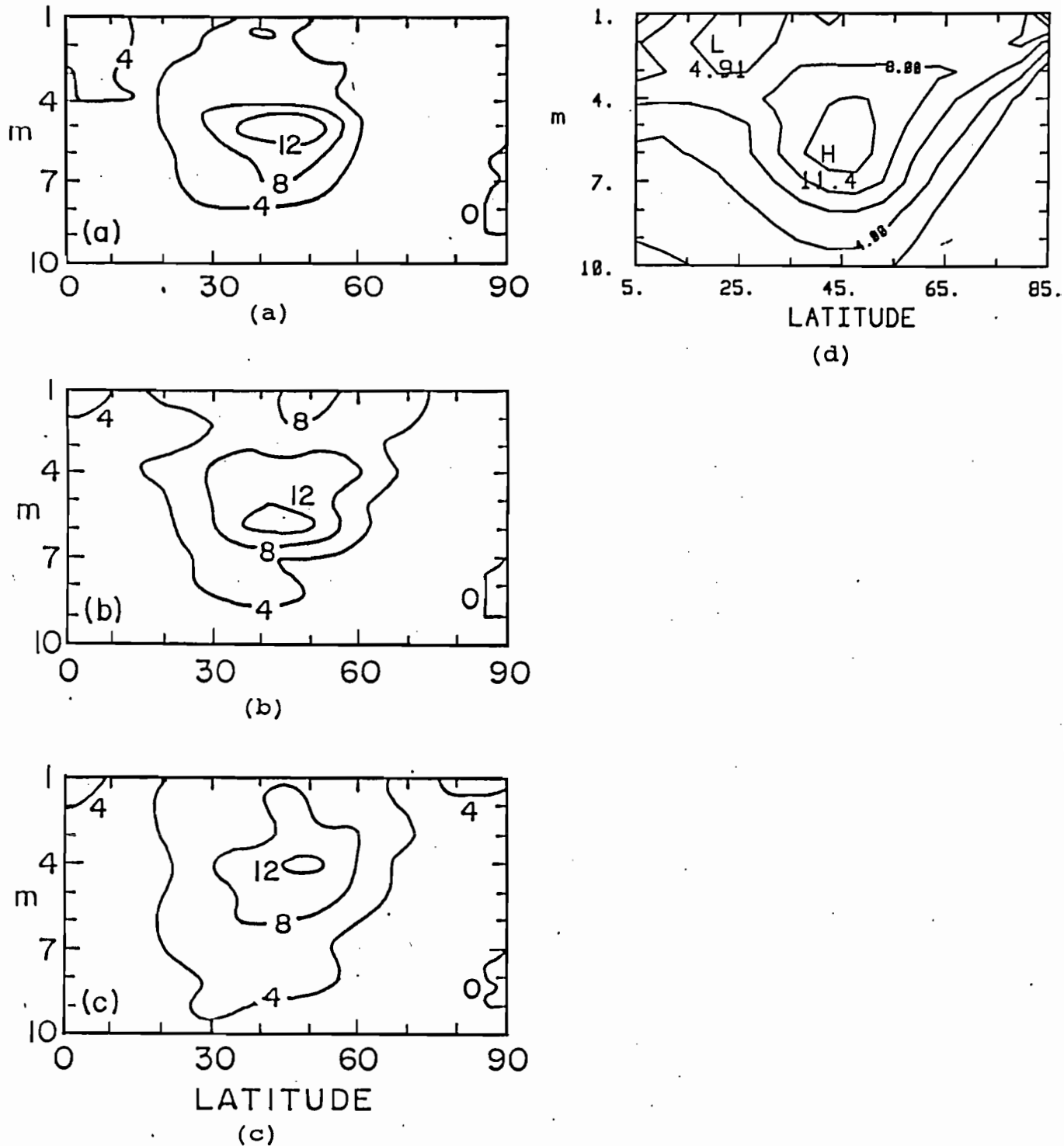


Figure 3.8: The zonal wavenumber-latitude distributions of the zonal and height integrated EKE, in units of 10^4 J m^{-2} . (a) January 1979, (b) February 1983, and (c) March 1983; all from NMC analyses (Lambert, private communication). (d) The model simulated EKE for DJF of years 2-7.

wavenumber/latitude EKE distribution obtained from NMC analyses for 3 different months: January 1979, February 1983, and March 1983. There is in each case a clearly defined EKE maximum in the medium scale wave regime: $m=5, 6, 4$ respectively for the 3 months. The maxima are all located between 45° - 50° S. For comparison, the model EKE distribution for DJF of years 2-7 are shown in Figure 3.8(d). The distribution shows a well defined maximum in wavenumbers $m=4-6$ at latitude 45° S. The magnitude and latitude of the maximum compare well with the observed values, with the model maximum being a bit weaker. The EKE distribution is almost entirely accounted for by the TE component, i.e., the SE contribution is small. The results for each of the 6 individual summers are summarized in Table 3.1. There is an interannual variation in the dominant wavenumber within the range of medium scale waves. This vacillation among different wavenumbers is also present in the observations, as seen from Figures 3.8(a)-(c). The interannual variability of the simulated EKE maxima and its latitude are in fairly good agreement with those of the observations.

Lambert (1986) computed the zonal wavenumber distribution of the horizontally and vertically averaged tropospheric EKE for January 1979, and C87 also calculated the wavenumber distribution for the eddy available potential energy (EAPE). Figure 3.9 shows the corresponding distributions for the years 2-7 model climatology of EKE and EAPE; the observed values for the summer of 1979 are also included. As noted already, most of the model EKE kinetic energy is due to the transient eddies. The model EKE distribution

year	wavenumber	EKE maximum	latitude
2	5	13.1	46°S
3	6	12.2	44°S
4	6	13.6	46°S
5	5	10.6	44°S
6	6	13.7	43°S
7	6	9.5	44°S
2-7	5	11.3	47°S

Table 3.1: The dominant zonal wavenumber of the wavenumber-latitude EKE spectrum of the CCC GCM, together with the magnitude of the maximum (10^4 J m^{-2}) and its latitude. Years "2-7" denotes the 6-year model climatology.

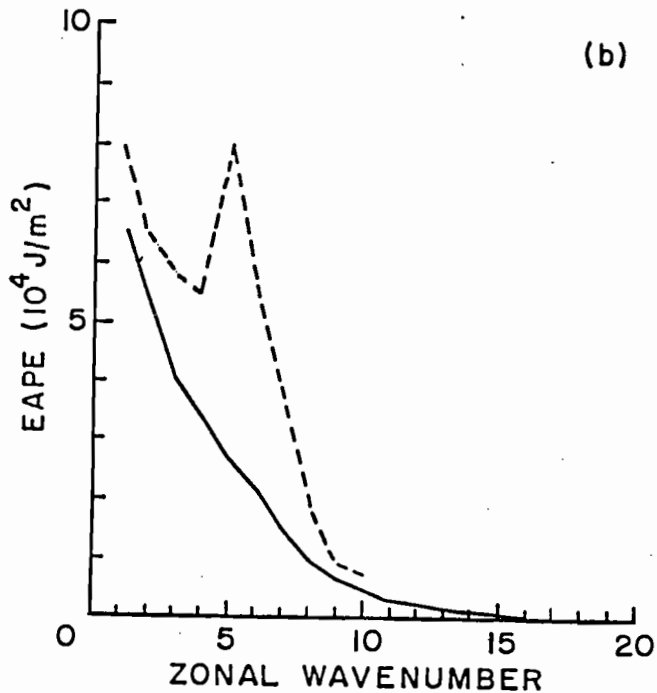
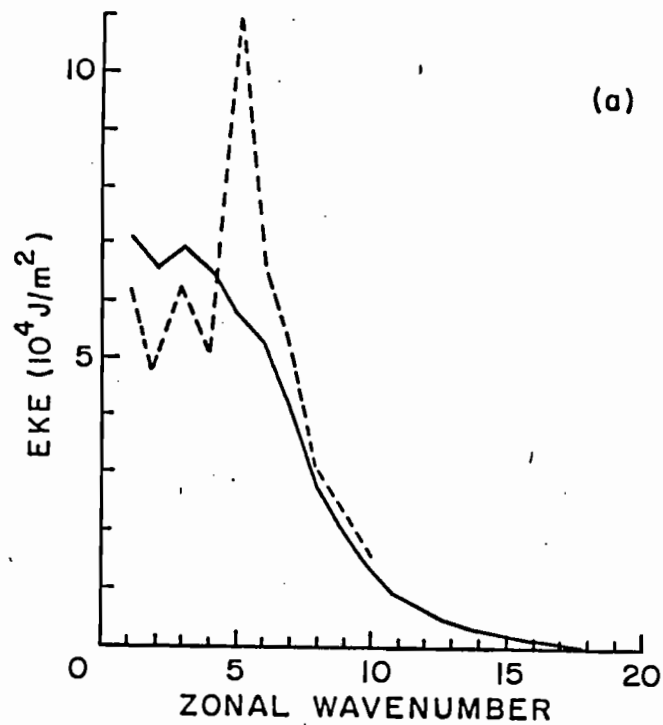


Figure 3.9: The zonal wavenumber distribution of EKE (a), and EAPE (b) integrated from 5°S - 85°S , 1000-150 mb, for DJF of years 2-7 (solid). The observed distributions for summer of 1979 (January 1979 for EKE from Lambert, 1986; DJF 1979 for EAPE of C87) are shown as the dashed lines.

shows more kinetic energy at the lower wavenumbers, and less at the medium scale waves, when compared to the January 1979 values. The EKE latitude-wavenumber distribution shows that lower wavenumbers(1-3) have very strong energy in high latitudes(>65S). This may be one reason explaining why the medium waves don't show a peak in Figure 3.9. However, the latter are only for one month, and may not be representative of the observed climatology, as a result of interannual variability. The model EAPE distribution is uniformly weaker than that observed for all zonal wavenumbers, and the observed peak in the medium scale wave is not reproduced.

The total EKE and EAPE, summed over zonal wavenumbers $m=1-20$, are shown in Table 3.2, for years 2-7. The observed values for DJF 1979 from C87 and their standard deviations are also included. Both the model energies are weaker than that observed for 1979, a result which is anticipated from the zonal wavenumber distributions discussed earlier. Also as noted already, the TE's account for most of the eddy energy in the model simulation.

In this section, we have examined the Southern Hemisphere medium scale wave regime as simulated by the CCC GCM. The propagation characteristics, latitudinal distribution and eddy kinetic energy spectra are diagnosed and compared with results of observational studies. The reasonable agreement shows that the model is quite successful at reproducing this wave regime, although the simulated regime tends to be weaker than that observed. In the next section, we continue the diagnosis with an examination of the eddy transports and energetics.

year	EKE	EAPE
2	53.1 (49.4)	29.9 (29.8)
3	52.8 (47.9)	28.1 (27.9)
4	51.2 (47.1)	27.7 (27.6)
5	49.8 (45.5)	28.4 (28.3)
6	51.9 (46.7)	29.2 (29.1)
7	50.2 (44.3)	28.5 (27.4)
2-7	51.5 (46.8)	28.5 (28.4)
C87	79.1 ± 13.7	48.6 ± 8.4

Table 3.2: The total EKE and EAPE for DJF of years 2-7, and observed values from C87. The TE contributions to the total eddy energies are shown in brackets. The observed values from C87 also include the standard deviations over the period DJF 1979. The unit is 10^4 J m^{-2} .

Chapter 4. Eddy transports and energetics

4.1 Zonally averaged heat and momentum transport

We have noted that results of observational studies suggest the medium scale waves are due to a finite amplitude baroclinic instability, with a sharp scale selection mechanism in both space and time. Moreover, the wave energetics show the classic life cycle of a baroclinic mode, characterized by baroclinic growth and barotropic decay. In this section, we examine the model simulated eddy heat and momentum transports, and the associated baroclinic and barotropic energy conversions. The vacillation cycle of the mean zonal flow as measured by the Richardson number, will also be investigated.

Figures 4.1(a) shows the latitude-pressure distribution of the eddy meridional heat transport, from the study of C87 of the observed eddy statistics of DJF 1979. There is a double maxima structure on the vertical plane, with the lower and upper tropospheric maxima being of comparable magnitudes. The filtered component corresponding to the medium scale waves ($m=4-6$; not shown) also has this vertical structure, with about a factor of two decrease in magnitudes. Lin and Chan (1989) examined the linear baroclinic instability of the 2-dimensional latitude-height January 1979 zonal wind using a quasi-geostrophic β -plane model. The latitude-height structure of the eddy heat transport for the $m=5$ mode shows a maximum at 50°S , close to latitude of the observed maximum. However, the vertical structure shows only a single maximum located near the ground, unlike that of the observations as shown in Figure 4.1(a). This vertical structure problem of linear

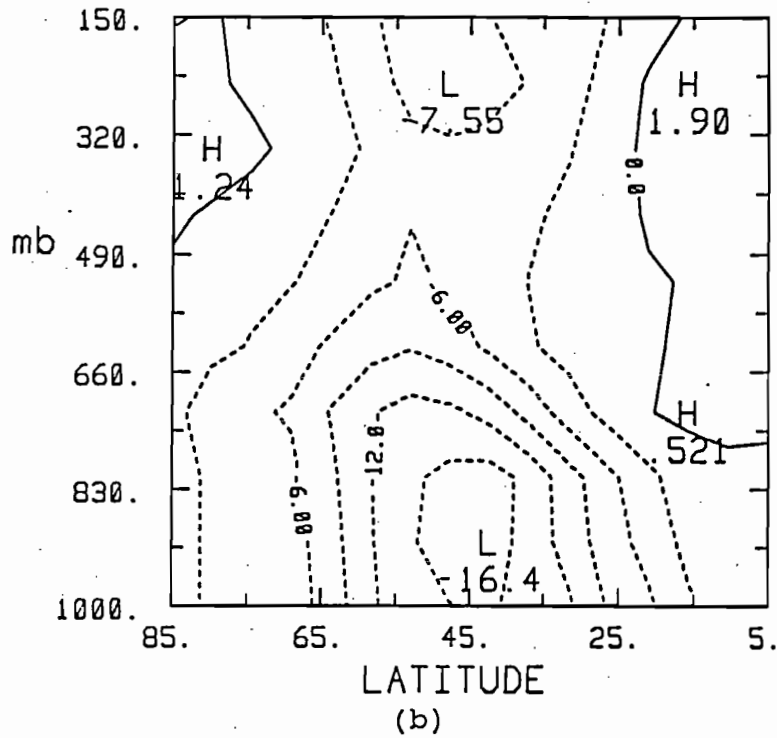
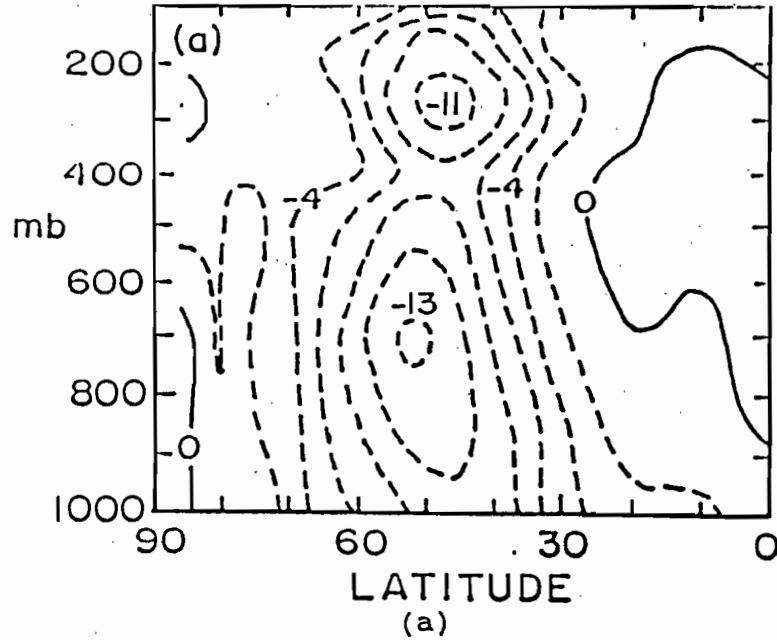


Figure 4.1: The zonally averaged meridional eddy heat transport ($K m s^{-1}$) on the latitude-pressure plane. (a) Observed values for DJF 1979, taken from C87. (b) The model climatology for DJF of years 2-7. Negative values indicate poleward transport.

baroclinic waves has been attributed to the linearization assumption (Gall, 1976; Frederiksen, 1981). The results of the CCC GCM shows that this may indeed be the case. Figure 4.1(b) shows the eddy meridional heat transport as simulated by the GCM, for DJF of years 2-7. There is now a double maximum in the vertical structure, in agreement with the observations. However, the magnitude of the upper tropospheric maximum is smaller than that observed, while the maximum near the surface is stronger than that of the observations. The latitudinal positions of the eddy maxima are also well simulated by the model.

C87 showed that the eddy transport of westerly momentum converges at the 50° - 60° S latitude band (Figure 4.2(a)), with the zonal wavenumbers $m=4-6$ accounting for about half of the total transport. The model eddy momentum transport is shown in Figure 4.2(b). The total eddy transport is smaller than that observed by almost a factor of two. Both the height and latitude of the momentum convergence zone are reproduced well by the model climatology. Again, we note that the observed results are for only one summer season.

We next examine the interannual variability of the meridional eddy heat and momentum transports of the model, for years 2-7 of the model simulation. The latitude-height structure of the transports of each individual year is quite similar to that of the 6-year climatology, the magnitudes do however vary. Table 4.1 shows the amplitudes of the lower and upper tropospheric heat transport maxima, and of the mid and high latitude maxima of the

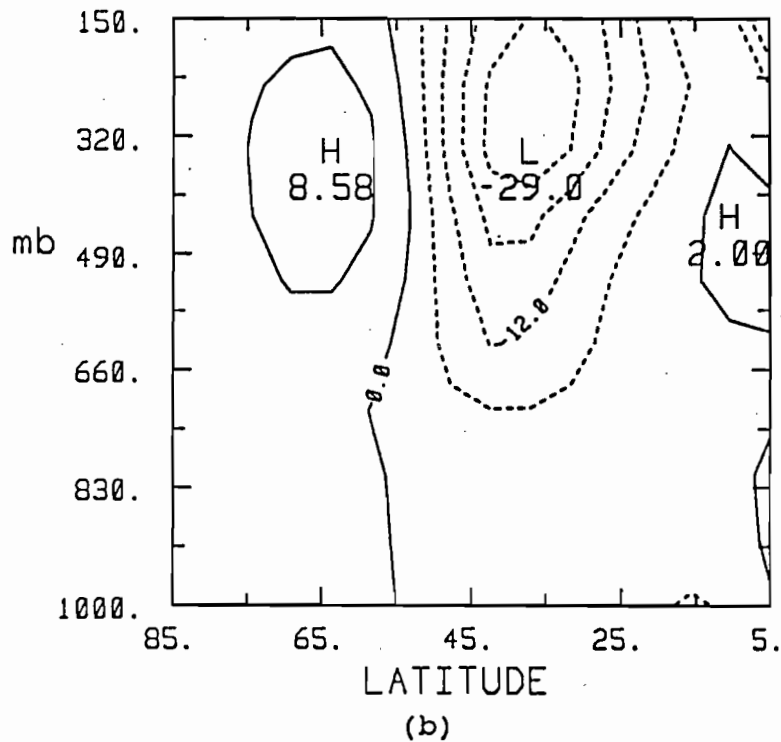
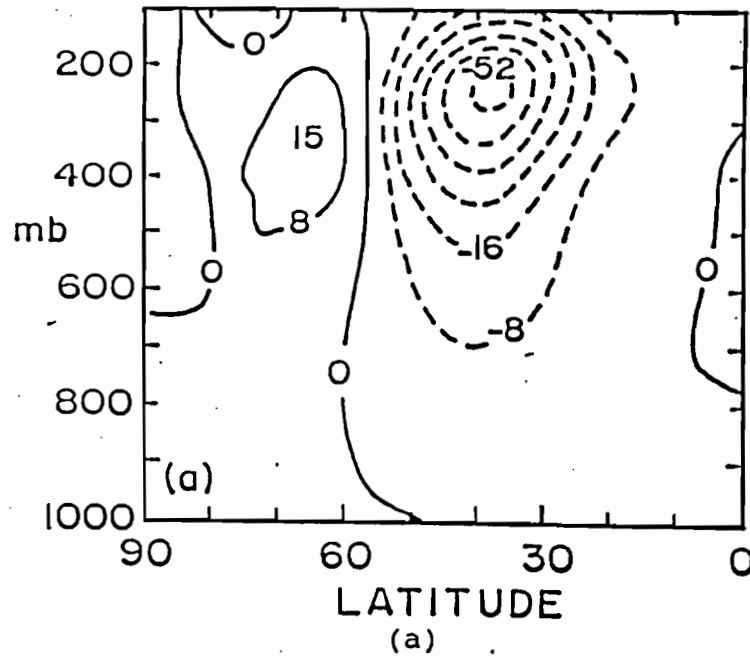


Figure 4.2: As Figure 4.1, but for the meridional eddy transport of westerly momentum ($m^2 s^{-2}$).

year	$[\langle v'T' \rangle]$	$[\langle u'v' \rangle]$
2	-16.6, -9.3 K m s ⁻¹	-40.2, 6.7 m ² s ⁻²
3	-16.4, -8.5	-32.5, 10.9
4	-16.7, -8.3	-36.6, 7.7
5	-16.0, -6.1	-15.3, 12.0
6	-16.4, -7.9	-32.3, 10.7
7	-16.6, -6.5	-23.8, 10.9
2-7	-16.4, -7.6	-29.0, 8.6
C87	-13, -11	-52, 15

Table 4.1: The amplitudes of the lower and upper tropospheric maxima of the meridional eddy heat transport ($[\langle v'T' \rangle]$), and of the mid and high latitude momentum transport ($[\langle u'v' \rangle]$), for model years 2-7 and observed values from C87. Negative values indicate poleward transport.

momentum transport from years 2-7. The values for the 6-year model climatology and the observational results of C87 are also shown. The heat transport shows a larger lower tropospheric maximum than the observations, while the upper tropospheric maximum is smaller, for each of the 6 years. The summer 1979 observations thus show a more barotropic vertical structure. There is little interannual variability in the amplitudes of the simulated transport. In contrast, the momentum transport shows considerable interannual variability. The magnitude of the poleward transport at mid-latitude varies by almost a factor of 3, while the equatorward transport at the high latitude ranges over a factor of almost 2. However, the model transports are consistently weaker than the observed values of summer 1979. We can thus conclude that the vertical tilt of the geopotential surfaces is better simulated than the horizontal tilt by the model.

4.2 Baroclinic and barotropic eddy conversions

The eddy heat and momentum transports play a major role in the baroclinic growth and barotropic decay of baroclinic planetary waves. This life cycle is characterized by the energy conversions ZAPE→EAPE→EKE→ZKE. The contributions of the TE's and SE's to these conversions are evaluated in this section.

$$C(\text{ZAPE}, \text{EAPE}) = C(\text{ZAPE}, \text{TEAPE}) + C(\text{ZAPE}, \text{SEAPE})$$

$$C(\text{EAPE}, \text{EKE}) = C(\text{TEAPE}, \text{TEKE}) + C(\text{SEAPE}, \text{SEKE})$$

$$C(\text{EKE}, \text{ZKE}) = C(\text{TEKE}, \text{ZKE}) + C(\text{SEKE}, \text{ZKE})$$

The notation used is standard; expressions for all the conversion terms are shown in the Appendix. The conversion $C(\text{ZAPE}, \text{EAPE})$ describes the release of ZAPE due to the eddy meridional heat transport down the gradient of mean temperature; this conversion can in turn be partitioned into the TE and SE components associated with the TE and SE heat flux respectively. $C(\text{EAPE}, \text{EKE})$ is the conversion to EKE associated with the sinking of colder air and rising of warmer air at different longitudes. It is made up of TE and SE components as well. $C(\text{ZAPE}, \text{EAPE})$ and $C(\text{EAPE}, \text{EKE})$ are the baroclinic energy conversions, representing the conversion of ZAPE to EKE. Finally, the barotropic decay term is the conversion of EKE to ZKE, associated with the eddy meridional momentum transport up the gradient of mean angular velocity. It can again be written as the sum of TE and SE components.

We now examine the zonal wavenumber distributions of the conversion terms computed for the model year 2-7 climatology, and compare the results to the observed values in DJF 1979 given by C87. Figure 4.3(a) shows $C(\text{ZAPE}, \text{EAPE})$ as a function of the zonal wavenumber. The conversion is almost totally accounted for by TE's, i.e., the SE contribution is small. There is a prominent peak near $m=5$ for the model climatology, as well as for the individual years (not shown). The maximum amplitude of the conversion for the model climatology near $m=5$ is about a factor of 2 smaller than that observed in 1979 by C87.

The total eddy component of the conversion $C(\text{EAPE}, \text{EKE})$ as well as that due to TE's are shown in Figure 4.3(b). The model results show that although the TE's remain the dominant

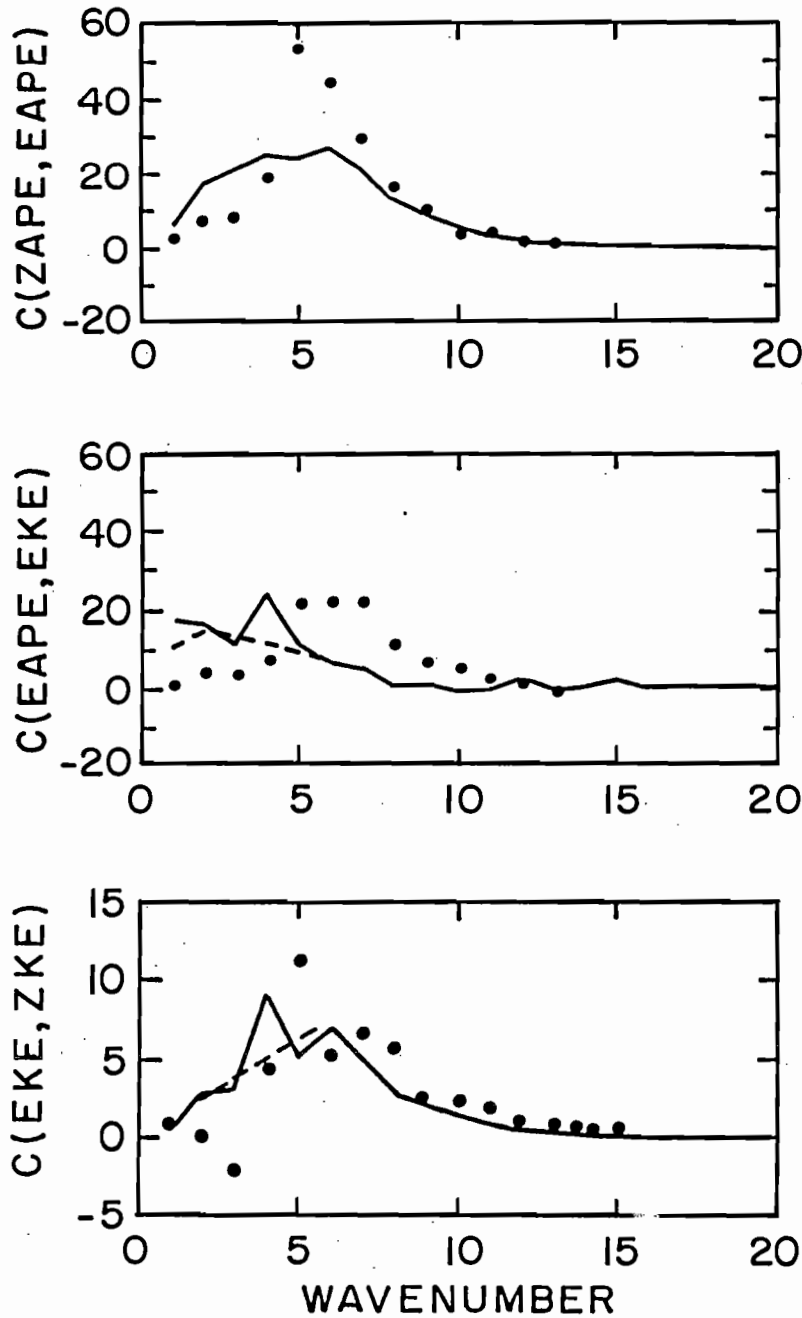


Figure 4.3: The model eddy conversions (10^{-2} W m^{-2}) integrated from 10° - 82° S, 1000-150 mb for years 2-7, as a function of the zonal wavenumber (m). (a) $C(\text{ZAPE}, \text{EAPE})$; (b) $C(\text{EAPE}, \text{EKE})$; and (c) $C(\text{EKE}, \text{ZKE})$. The solid and dashed lines denote the total eddy and TE contributions respectively, while the dots are observed values for DJF 1979, from C87. The dashed line is not shown in (a) as it is indistinguishable from the solid line.

component in the total eddy conversion, the SE's are also important, especially at zonal wavenumbers $m=1$ and $m=4$. In contrast, the observed values show a broad peak at smaller zonal scales corresponding to $m=5-7$.

The zonal wavenumber spectra of the barotropic conversion $C(EKE, ZKE)$ due to TE's and SE's, and due to TE's only, are shown in Figure 4.3(c). The SE contribution is small, except at zonal wavenumbers $m=4$. This is consistent with our earlier finding that the stationary zonal variance is concentrated at $m=1$ and $m=3$. The maximum eddy conversion at the medium scales present in the observations of C87 is simulated, but with weaker amplitudes. However, we note that this conversion is the smallest of the three conversions examined.

A comparison of the total eddy conversions, summed over zonal wavenumbers, is shown in Table 4.2. The corresponding observed values of C87 are also shown. It is clear that the model energy conversions tend to be smaller than those observed during DJF 1979. Nonetheless, there is reasonable agreement for the two baroclinic conversions, $C(ZAPE, EAPE)$ and $C(EAPE, EKE)$. TE's account for practically all of the baroclinic conversion $C(ZAPE, EAPE)$, while SE's become important for $C(EAPE, EKE)$ and $C(EKE, ZKE)$. There is much more interannual variability in the two conversions, $C(EAPE, EKE)$ and $C(EKE, ZKE)$ than in the baroclinic conversion $C(ZAPE, EAPE)$.

In a linear β -plane quasi-geostrophic baroclinic instability analysis, Lin and Chan (1989) computed the Richardson number (Ri) of the basic state using the zonally averaged January 1979

year	C(ZAPE, EAPE)	C(EAPE, EKE)	C(EKE, ZKE)
2	189.2 (189.1)	82.2 (60.7)	54.6 (48.0)
3	178.1 (178.0)	120.7 (90.3)	35.8 (33.6)
4	179.2 (179.1)	89.9 (64.5)	44.0 (36.8)
5	151.2 (151.1)	70.8 (54.9)	25.2 (21.2)
6	167.1 (166.9)	108.8 (69.3)	49.2 (38.8)
7	159.1 (159.0)	99.4 (75.8)	29.1 (25.7)
2-7	170.6 (170.5)	95.3 (69.2)	39.6 (34.0)
C87	204 ± 90	122 ± 53	42 ± 66

Table 4.2: Energy conversions for model years 2-7, and observed values from C87. The later include the standard derivation over the period DJF 1979. The TE contributions to the total eddy conversion are shown in brackets. The unit is 10^{-2} W m^{-2} .

potential temperature and zonal wind fields.

$$Ri = [-\rho^{-1}(\ln [\theta])_p]/[U]_p^2$$

Here, ρ , p , $[\theta]$, $[U]$ are the density, pressure, zonally averaged basic state potential temperature, and basic zonal wind respectively. Subscripts denote partial differentiation. The Richardson number is thus a measure of the baroclinicity of the basic state, as it provides an estimate of the relative effects of the static stability and the vertical wind shear. Lin and Chan showed that there is a minimum in Ri associated with the January 1979 zonally averaged tropospheric circulation. This is in term corresponds to the growth of baroclinic waves on this basic state. We now examine the Richardson number distribution as simulated by the model.

The zonally averaged distributions of temperature, zonal wind, and the corresponding Richardson number for years 2-7 are shown in Figure 4.4. The model climatology shows a temperature and zonal wind field in thermal wind balance, with the maximum latitudinal temperature gradient located at mid-latitudes, where the vertical shear of the zonal wind is maximum. The Richardson number field shows two minima in the troposphere between 35° and 45° S. The primary minimum of $Ri=14.9$ is reached in the upper troposphere; this corresponds to where the medium scale waves attain the largest amplitude. Examination of the individual years of the model simulation shows that the minimum Ri does not exceed 20.

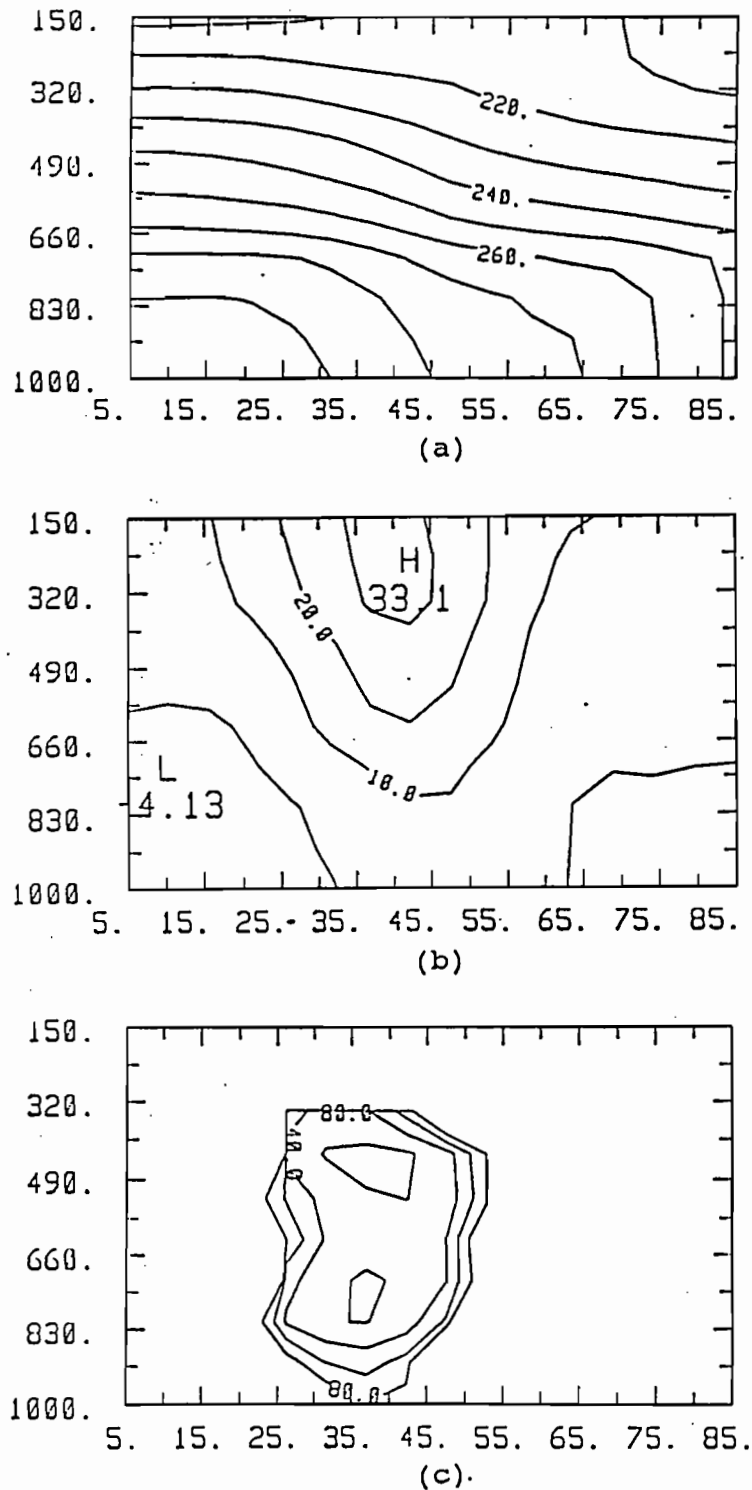


Figure 4.4: The zonally averaged distributions of (a) temperature (K), (b) zonal wind ($m s^{-1}$), and (c) Richardson number (Ri), for DJF of years 2-7, values of Ri > 80 are not shown.

C87 examined the time series of eddy energies and eddy energy conversions, and found that the medium scale waves showed a clear vacillation period of 2 weeks. Baroclinic processes are important in the maintenance of this vacillation. As the Richardson number is a measure of the baroclinicity of the mean zonal flow, it is of interest to examine the time variation of this parameter. Figure 4.5 shows the time series for the upper tropospheric Ri minima, for DJF of model year 2. We see there is significant variation of Ri over this period; there are 8 vacillation peaks in this 90-day period, giving a vacillation period of about 11 days. This agrees with the results of C87. Examination of the time series for the model EKE and baroclinic energy conversion $C(ZAPE, EAPE)$ (not shown) also reveal a similar vacillation period.

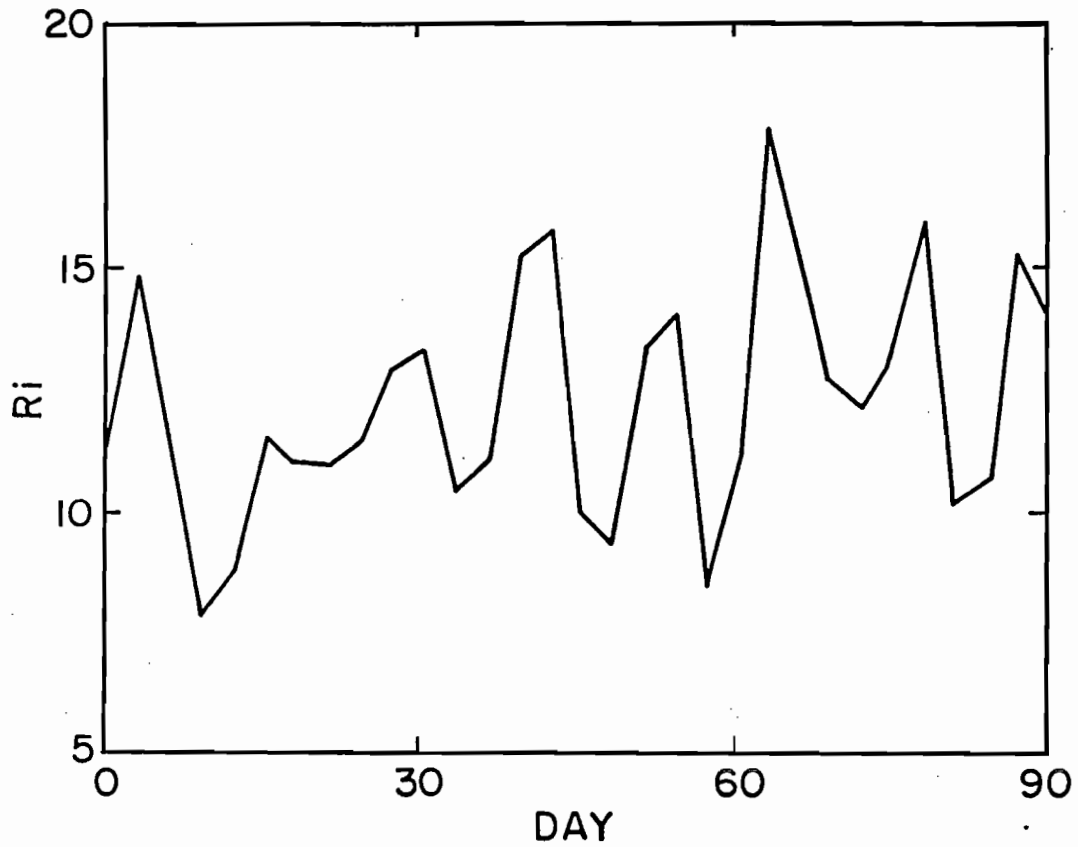


Figure 4.5: The time series for the upper tropospheric Richardson number (Ri) minima, for DJF of model year 2.

Chapter 5. Conclusions

We have examined the eddy statistics of the summer Southern Hemisphere tropospheric circulation as simulated by the Canadian Climate Centre general circulation model. The study is motivated by the presence of a strong zonal wavenumber $m=5$ signal in the observed circulation, which is well documented in the literature. In contrast, little modelling work has been done. The major conclusions of our study are discussed below.

1) An examination of various space-time power spectra, and zonal wavenumber spectra shows that the CCC GCM is able to simulate the observed medium scale planetary wave regime. The observed results used for comparison in this study is for the period DJF 1979, when a prominent wavenumber 5 signal dominates the circulation in the Southern Hemisphere.

The model climatology shows a clear signal in the medium scale waves with a period about 10 days, and peak amplitude at around 45°S , in good agreement with the observations. The stationary component is much weaker than the transient component. The zonal wavenumber vacillation among the wavenumbers $m=4-6$ observed in different months and years is also simulated as interannual variability of the model.

Xu et al. (1990) compared the performance of 4 GCM's in the Southern Hemisphere. The results showed that the CCC GCM performed better than the other models (NCAR, ECMWF, GFDL) in reproducing the annual cycle of the zonally averaged intensity and position of the subpolar trough. In particular, the trough is too shallow and displaced too far toward the mid-latitudes in the other models.

However, they did not examine the medium scale planetary wave regime. As evidence of this wave regime has not been reported in the literature using the other GCM's, it would be of great interest to perform similar diagnostic studies using these models.

2) The meridional eddy heat and momentum transports and the associated baroclinic and barotropic energy conversions are also examined. The simulated zonally averaged distributions of the heat and momentum transports agree reasonably well with those of DJF 1979 reported in the literature. Quantitative differences remain; the vertical structure of the meridional heat transport is too baroclinic, while the momentum transport tends to be too weak. Earlier studies with linear quasi-geostrophic models show that the $m=5$ wave is not the fastest growing mode, and its zonally averaged eddy structure bears only qualitative resemblance to the observed wave. The success of the GCM in simulating both the zonal scale selection and the eddy structure suggests that the medium scale wave is governed by nonlinear primitive equation dynamics.

The zonal wavenumber distributions of the baroclinic conversions $C(ZAPE, EAPE)$, and $C(EAPE, EKE)$, and the barotropic conversion $C(EKE, ZKE)$, all show a medium scale wave signal, in agreement with observations. The magnitudes of the conversions tend to be smaller than those observed.

3) Observational studies suggest that the medium scale wave is a finite amplitude baroclinic instability, with a life cycle consisting of baroclinic growth and barotropic decay characteristic of baroclinic waves. The Richardson number Ri is a measure of the baroclinicity of the zonal flow. The time evolution of Ri over a

90-day period shows that high values of R_i reveals a vacillation time scale of 11 days, in good agreement with observed results. It is thus likely that the R_i distribution of the zonal flow plays an important role in the life cycle of the medium scale wave.

Appendix

We give here the expressions used in the various energy conversion terms. The notation and formulation are similar to that of Peixóto and Oort (1974).

a	average radius of the earth;
C_p	specific heat at constant pressure;
$C(P, K)$	conversion rate of P into K;
dm	mass element, equal to $a^2 \cos \phi d\lambda d\phi dp/g$;
dx	$a \cos \phi d\lambda$;
dy	$a d\phi$;
g	acceleration resulting from gravity;
K	kinetic energy;
ZKE, EKE	zonal, eddy kinetic energy;
TEKE, SEKE	transient, stationary eddy kinetic energy;
p	pressure;
P	available potential energy;
ZAPE, EAPE	zonal, eddy available potential energy;
TEAPE, SEAPE	transient, stationary eddy available potential energy;
R	gas constant;
t	time;
T	temperature;
u	zonal wind component;
v	meridional wind component;
Z	geopotential height;

γ stability factor,

$$-(\theta/T) (R/C_p P) \left(\frac{\partial[\langle\theta\rangle]}{\partial P} \right)^{-1} = \Gamma_d [\langle T \rangle]^{-1} (\Gamma_d - [\langle T \rangle])^{-1};$$

Γ lapse rate $-\partial T/\partial z$;

Γ_d dry adiabatic lapse rate g/C_p ;

θ potential temperature $T(1000/P)^{R/C_p}$;

κ R/C_p ;

λ geographic longitude;

ϕ geographic latitude;

$\langle A \rangle$ time average of A, $(t_2 + t_1) / \int_{t_1}^{t_2} A dt$;

A' departure from zonal average of A, $A - \langle A \rangle$;

$[A]$ zonal average of A, $(2\pi)^{-1} \int_0^{2\pi} A d\lambda$;

A^* departure from zonal average of A, $A - [A]$;

\bar{A} meridional average of A, $\int_0^{\pi/2} A \cos\phi d\phi$;

A'' deviation from meridional average of A, $A - \bar{A}$.

The expression for the various forms of energy are defined as:

$$E_{APE} = T_{E_{APE}} + S_{E_{APE}}$$

$$T_{E_{APE}} = \frac{C_p}{2} \int_{\gamma} [\langle T'^2 \rangle] dm$$

$$S_{E_{APE}} = \frac{C_p}{2} \int_{\gamma} [\langle T''^2 \rangle] dm$$

$$EKE = TEKE + SEKE$$

$$TEKE = \frac{1}{2} \int [(\dot{u}^2) + (\dot{v}^2)] dm$$

$$SEKE = \frac{1}{2} \int [(\dot{u}^{*2}) + (\dot{v}^{*2})] dm$$

$$C(ZAPE, EAPE) = C(ZAPE, TEAPE) + C(ZAPE, SEAPE)$$

$$C(ZAPE, TEAPE) = -C_p \int \gamma [(\dot{v}'T')] \frac{\partial [(T)']}{a \partial \phi} dm$$

$$C(ZAPE, SEAPE) = -C_p \int \gamma [(\dot{v}^*T^*)] \frac{\partial [(T)']}{a \partial \phi} dm$$

$$C(EAPE, EKE) = C(TEAPE, TEKE) + C(SEAPE, SEKE)$$

$$C(TEAPE, TEKE) = - \int g \left(\left[\left(\frac{u' \partial Z'}{a \cos \phi \partial \lambda} \right) + \left(\frac{v' \partial Z'}{a \partial \phi} \right) \right] \right) dm$$

$$C(SEAPE, SEKE) = - \int g \left(\left[\left(\frac{\dot{u}^* \partial Z^*}{a \cos \phi \partial \lambda} + \frac{\dot{v}^* \partial Z^*}{a \partial \phi} \right) \right] \right) dm$$

$$C(EKE, ZKE) = C(TEKE, TEAPE) + C(ZAPE, SEAPE)$$

$$C(EKE, ZKE) = \int [(\dot{v}'u')] \cos \phi \left\{ \frac{\partial [(u)'] / \cos \phi}{a \partial \phi} \right\} dm$$

$$+ \int (\dot{v}^2) \frac{\partial [(v)']}{a \partial \phi} dm$$

$$- \int [(\dot{v})] [(\dot{u}^2)] \frac{\tan \phi}{a} dm$$

$$\begin{aligned}
C(SEKE, ZKE) &= \int [(\nu)^*(u)^*] \cos\phi \left\{ \frac{\partial([\omega]/\cos\phi)}{a\partial\phi} \right\} dm \\
&+ \int [(\nu)^*(u)^*] \frac{\partial[(\nu)]}{a\partial\phi} dm \\
&- \int [(\nu)] [(u)^*(u)^*] \frac{\tan\phi}{a} dm
\end{aligned}$$

Reference

- Bjørheim, K., P. Julian, M. Kanamitsu, P. Kållberg, P. Price, S. Tracton and S. Uppala, 1981: FGGE III-B Daily Global Analyses, Part 1, December 1978 - February 1979. The Global Weather Experiment. European Centre for Medium Range Weather Forecasts.
- Boer, G.J., N.A. Mcfarlane, R. Laprise, J.D. Henderson and J.P. Blanchet., 1984a: The Canadian Climate Centre spectral atmospheric general circulation model. *Atmos.-ocean*, **22**, 397-429.
- _____, _____ and _____, 1984b: The climatology Canadian Climate Centre spectral general circulation model as obtained from a five years simulation. *Atmos.-Ocean*, **22**, 430-473.
- Chen, T.C., M.C.Yen and D.P.Nune, 1987: Dynamic aspects of the Southern-Hemisphere medium-scale waves during the southern summer season. *J. Meteor. Soc. Japan*, **65**, 401-420.
- Hamilton, K., 1983: Aspects of wave behaviour in the mid- and upper troposphere of the southern hemisphere. *Atmos.-Ocean*, **21**, 40-54.
- Hayashi, Y., 1982: Space-time spectral analysis and its applications to atmospheric waves. *J. Meteor. Soc. Japan*, **60**, 156-171.
- Kalnay, E., K.C. Mo and J. Peagle, 1986: Large-amplitude, short-scale stationary rossby waves in the Southern Hemisphere: Observation and Mechanistic experiments to Determine their origin. *J. Atmos. Sci.*, **43**, 252-275.

- Lambert, S.J., 1986: A study of the kinetic energy of the Southern Hemisphere during January and July with emphasis on the FGGE year. *Tellus*, **38A**, 429-438.
- Lin, C.A., and A.C.M., Chen, 1989: Baroclinic instability and the summer Southern Hemisphere wavenumber 5 circulation. *Geophys. Astrophys. Fluid Dynamics.*, **47**, 19-42.
- Peixoto, J.P., and A.H.Oort, 1974: The annual distribution of the atmospheric energy on a planetary scale. *J. Geophys. Res.*, **79**, 2149-2159.
- Randel, W.J., and J.L. Stanford, 1983: Structure of medium-scale atmospheric waves in the Southern Hemisphere summer. *J. Atmos. Sci.*, **40**, 2312-2318.
- _____, and _____, 1985a: An observational study of medium-scale wave dynamics in the Southern Hemisphere summer. Part I: Wave structure and energetics. *J. Atmos. Sci.*, **42**, 1172-1188.
- _____, and _____, 1985b: An observational study of medium-scale wave dynamics in the Southern Hemisphere summer. Part II: Stationary-transient wave interference. *J. Atmos. Sci.*, **42**, 1189-1197.
- _____, and _____, 1985c: The observed life cycle of a baroclinic instability. *J. Atmos. Sci.*, **42**, 1364-1373.
- Salby, M.L., 1982: A ubiquitous wavenumber-5 anomaly in the Southern Hemisphere during FGGE. *Mon. Wea. Rev.*, **110**, 1172-1188.

Xu, J.S., H.V. Storch, and H.V. Loon, 1990: The performance of four spectral GCMs in the Southern Hemisphere: The January and July climatology and the semi-annual wave. *J. Climate*, 3, 53-70.